Journal of Power Sources 283 (2015) 181–186

Contents lists available at ScienceDirect

Journal of Power Sources

journal homepage: www.elsevier.com/locate/jpowsour

Kinetics of the hydrogen oxidation reaction on nanostructured rhodium electrodes in alkaline solution

María A. Montero, María R. Gennero de Chialvo, Abel C. Chialvo*

Programa de Electroquímica Aplicada e Ingeniería Electroquímica (PRELINE), Facultad de Ingeniería Química, Universidad Nacional del Litoral, Santiago del Estero 2829, 3000 Santa Fe, Argentina

HIGHLIGHTS

- Kinetic study of the hydrogen oxidation reaction in alkaline solution.
- Nanostructured rhodium supported on glassy carbon.
- Experimental polarization curves at different rotation rates.
- Tafel-Heyrovsky-Volmer mechanism and Frumkin type adsorption.
- Reaction proceeds mainly through the Tafel-Volmer route.

ARTICLE INFO

Article history:
Received 23 December 2014
Received in revised form
21 February 2015
Accepted 23 February 2015
Available online 25 February 2015

Keywords:
Hydrogen oxidation reaction
Rhodium electrode
Alkaline solution

ABSTRACT

The hydrogen oxidation reaction was studied on a nanostructured rhodium electrode at different rotation rates in alkaline solution. The electrode was prepared via sputtering on a glassy carbon disc support and it was characterized by atomic force microscopy and cyclic voltammetry. The real surface area was evaluated by CO stripping voltammetry. Experimental current density (j) – overpotential (η) curves of the hydrogen oxidation reaction were obtained in the range $-0.015 \leq \eta/V \leq 0.40$ at different rotation rates ($900 \leq \omega/rpm \leq 4900$). The resulting curves were correlated by kinetic expressions derived from the Tafel-Heyrovsky-Volmer mechanism with a Frumkin type adsorption of the reaction intermediate and the kinetic parameters were evaluated. It was verified that over this overpotential region the reaction in alkaline solution proceeds mainly through the Tafel-Volmer route. These results were compared with those previously obtained in acid solutions.

1. Introduction

In the last decade there was a marked increase in the interest in the hydrogen oxidation reaction (hor), which led to numerous experimental studies on different electrode materials in acid solutions [1–8]. There was also advances in the derivation of theoretical expressions for the interpretation of the experimental dependences of the current density (j) on overpotential (η), under the kinetic mechanism of the Tafel-Heyrovsky-Volmer [9–11]. Starting from these equations, the kinetic parameters (equilibrium reaction rates of the elementary steps and equilibrium surface coverage) were evaluated on different noble metals [12–16]. Conversely, the hydrogen oxidation reaction in alkaline solution has not received similar attention, being scarce the published works [17–20]. In the particular case of rhodium electrodes, it cannot be found any kinetic study of the hydrogen oxidation reaction in alkaline medium. On this context, the present work deals with the evaluation of the elementary kinetic parameters of the Volmer-Heyrovsky-Tafel mechanism on nanostructured Rh electrodes through the correlation of experimental current density vs. overpotential curves, measured in 0.1 M NaOH solution under steady state and controlled mass transport conditions.

2. Experimental details

2.1. Electrode preparation and characterization

The working electrodes were prepared via sputtering on a glassy carbon substrate from a rhodium target in an argon atmosphere.

* Corresponding author.
E-mail address: achialvo@fiq.unl.edu.ar (A.C. Chialvo).

http://dx.doi.org/10.1016/j.jpowsour.2015.02.133
0378-7753/

The preparation details can be found elsewhere [16]. The surface morphology of the Rh electrodes was characterized by Atomic Force Microscopy (AFM). AFM images were obtained using a multitechnique Agilent microscope model 5400, operated in tapping mode and processed with the software WSxM 6.2.

The electrode was also characterized electrochemically by cyclic voltammetry carried out in a three electrodes cell. The electrolytic solution was 0.1 M NaOH (Merck pro analysis), prepared with ultrapure water (PureLab, Elga LabWater). The working electrode was mounted in a teflon holder, with an exposed geometric area of 0.07 cm^2 (A_g). Furthermore, a large area platinum wire acted as counter electrode, located externally to the cell to avoid contamination from platinum electrodissolution. A hydrogen electrode in the same solution (RHE) was used as reference electrode, placed in a holder connected to a Luggin capillary of 0.2 mm diameter, located in the centre and at a distance of 0.2 mm of the working electrode surface. This configuration ensures that the ohmic effects are negligible in the experimental conditions and that the hydrodynamics of the rotating electrode is not affected. Cyclic voltammetry was carried out using a potentiostat-galvanostat Wenking POS2 controlled by an interface Advantech PI1710HG and the software Labview 8. The voltammograms were obtained at 0.05 V s^{-1} in nitrogen saturated solution between 0.0 and 1.3 V.

The real area of the electrode was determined by carbon monoxide stripping voltammetry. CO adsorption was carried out in an auxiliary cell in a CO saturated solution of 0.5 M H_2SO_4 (Merck pro analysis) holding the electrode potential at 0.05 V (vs. RHE) during 15 min. Then, the voltammetric stripping was carried out at 0.05 V s^{-1} in nitrogen saturated solution between 0.05 and 1.3 V.

2.2. Hydrogen oxidation measurements

The experimental determination of the dependence $j(\eta)$ for the hydrogen oxidation reaction on steady state was carried out in the cell described above. Five rotating rates (ω) was employed in the range $900 \leq \omega/\text{rpm} \leq 4900$, using a rotating disc equipment (Radiometer EDI 10000). The electrolyte solution was NaOH 0.1 M, which was subjected to a continuous and efficient hydrogen bubbling at P = 1 atm. The counter electrode was a large area Pt electrode. The applied overpotential was varied in the range $-0.015 < \eta/\text{V} < 0.40$, controlled against a hydrogen electrode reference in the same electrolyte solution. A potential program was applied in order to obtain the steady state polarization curves. It was initiated with a 3 s step at 0.0 V, followed by a 5 s step to the desired overpotential value. In this last period, readings of the current value were made each 0.1 s and the mean value of the current data measured in the last 2 s was assigned to the step overpotential. Then the program was repeated for each η value. The electrolyte solution was renewed after each experiment, which were carried out at 25 °C.

3. Results and discussion

3.1. Electrode characterization and real area evaluation

Fig. 1 shows the voltammetric profile of the nanostructured Rh electrode in 0.1 M NaOH solution at 0.05 V s^{-1} under nitrogen bubbling in the potential range $0.0 < E/\text{V} < 1.3$ vs. RHE. It can be appreciated in the anodic scan the profile corresponding to the hydrogen desorption located between 0.1 and 0.3 V, immediately followed by the electroadsorption of OH and other rhodium hydroxylated species. The cathodic sweep shows the peak corresponding to the electroreduction of such species at approximately 0.37 V, which is strongly overlapped with the peaks corresponding to the hydrogen electroadsorption, due to the late disinhibition of

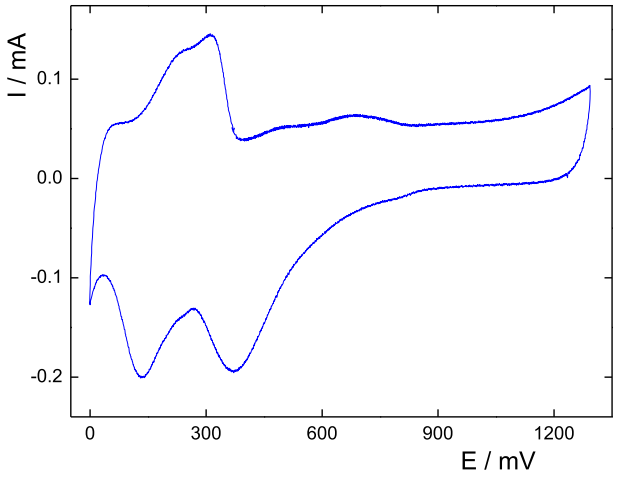

Fig. 1. Voltammogram of the Rh electrode in 0.1 M NaOH at 0.05 V s^{-1} and 298 K.

the adsorption sites occupied by the Rh oxide [21,22]. The potentiodynamic profile is similar to that corresponding to electrodeposit Rh in 1 M KOH solution [21].

The voltammetric charge corresponding to the electrooxidation of the adsorbed CO in acid solution was used for the determination of the real electrode area (Fig. 2). The first cycle corresponds to the stripping of the adsorbed CO, where it can be observed a sharp peak at approximately 0.725 V. The complete electrooxidation of the adsorbed CO is produced in this first anodic sweep, as it can be verified through the second voltammetric cycle, which reproduces the blank voltammogram of metallic rhodium in this electrolyte solution [16,23,24]. The voltammetric charge corresponding to the electrooxidation of the adsorbed CO was evaluated as the difference between the first and second cycle in the potential range $0.40 < E/\text{V} < 1.3$, resulting a value equal to 0.301 mC. Taking into account that the voltammetric charge of one CO monolayer is equal to 0.2877 mC cm^{-2} [16], the electroactive area (A_e) of the Rh electrode is 1.043 cm^2. Moreover, as the reaction under study has a strong diffusion contribution, which depends on the geometric area, meanwhile the kinetic reaction takes place on the real surface area, the relationship between both values is an important parameter for the correct analysis of the reaction. This relationship, called active area factor ($f_{aa} = A_e/A_g$), is in this case equal to 14.69.

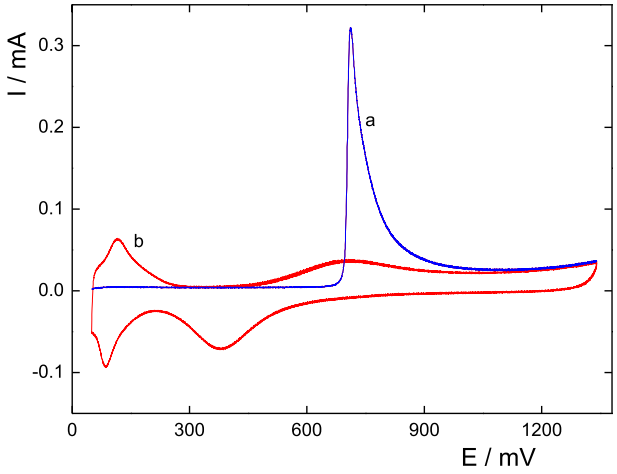

Fig. 2. Voltammetric stripping of adsorbed CO on the Rh electrode. (a) First cycle; (b) Second cycle. 0.05 V s^{-1}; 0.5 M H_2SO_4, 298 K.

3.2. Morphological characterization

Fig. 3 shows the surface morphology of the working electrode obtained by sputtering on a glassy carbon (GC) substrate. It can be observed from the AFM image that the Rh layer consists of nanoparticles with an average size of 70–80 nm. They are agglomerated in different levels. This result explains the high value of the active area factor obtained by CO stripping.

3.3. Hydrogen oxidation reaction

The current (I) on time (t) response of the Rh electrode resulting from the application of the potential program described in the Experimental section is shown in Fig. 4, for all the rotation rates analyzed (900, 1600, 2500, 3600 and 4900 rpm) and for the overpotentials range comprised between $-0.015 \leq \eta/V \leq 0.40$. It can be observed that current quickly reached the steady state condition. Moreover, in this overpotentials range it is not perceived the inhibition of the adsorption sites due to the adsorption of hydroxylated species, which takes place at higher overpotentials. Readings of the current value were made each 0.1 s and the mean value of the current data measured in the last 2 s was assigned to the step overpotential. Starting from these results and taking into account the real electrode area, the corresponding $j(\eta)$ dependences on steady state were evaluated for each rotation rate, which are shown in Fig. 5 (symbols). It can be observed that there is a marked influence of rotation. These experimental curves were correlated with the system of equations resulting from the resolution of the kinetic mechanism of Tafel-Heyrovsky-Volmer (TVH) on steady state,

$$H_2 + 2S \rightleftarrows 2H_{ad} \quad \text{Tafel} \tag{1-1}$$

$$H_2 + OH^- + S \rightleftarrows H_{ad} + H_2O + e^- \quad \text{Heyrovsky} \tag{1-2}$$

$$H_{ad} + OH^- \rightleftarrows H_2O + e^- + S \quad \text{Volmer} \tag{1-3}$$

where S represents a site on the electrode surface in which the reaction intermediate H_{ad} can be adsorbed. The THV mechanism

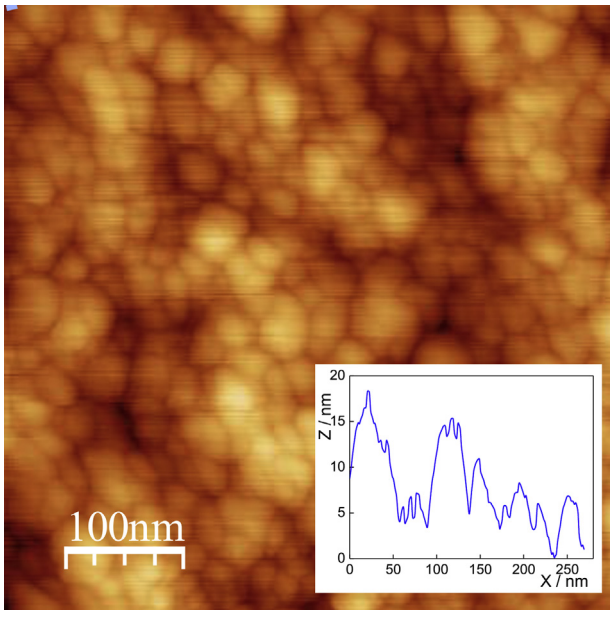

Fig. 3. AFM image of the nanostructured Rh electrode. Inset: height profile.

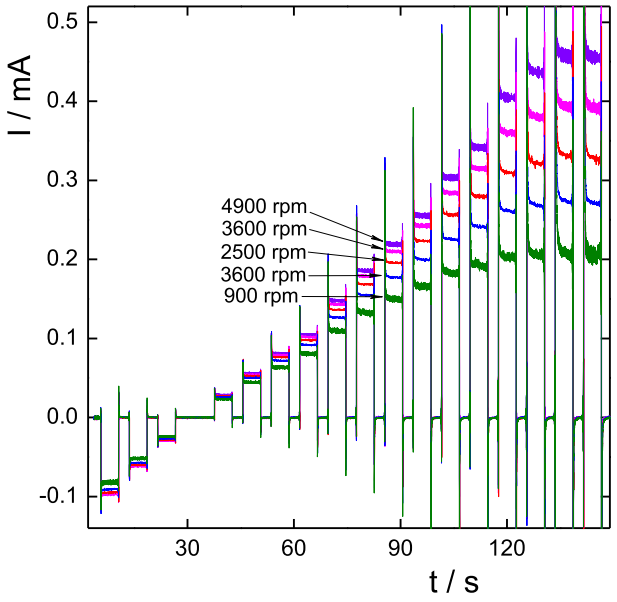

Fig. 4. Current vs. time response of Rh electrode to the overpotential program applied in the range -0.015 V $\leq \eta \leq$ 0.4 V at different rotation rates (indicated in the figure). 0.1 M NaOH; 298 K.

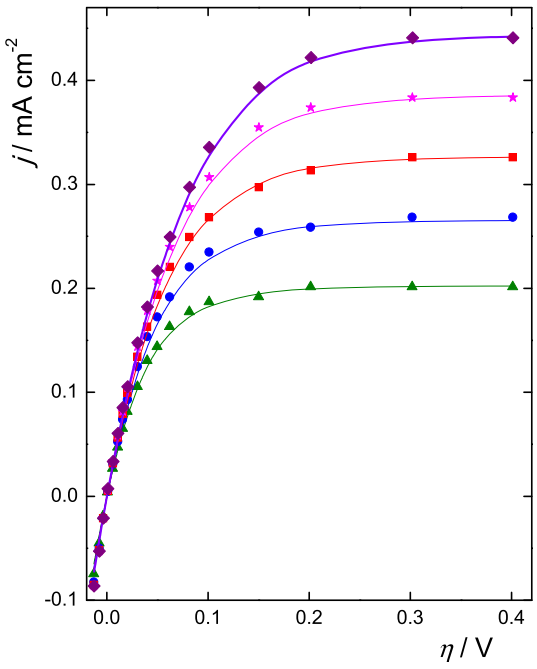

Fig. 5. Experimental (symbols) and simulated (lines) $j(\eta)$ curves of the *hor* on Rh electrode. 0.1 M NaOH; 298 K. ω = (▲) 900; (●) 1600; (■) 2500; (★) 3600; (◆) 4900 rpm.

establishes certain constrains, which are useful to validate its application. Thus, it must be verified a linear dependence of the inverse of the maximum value of the current density (j_{max}) and the inverse of the square root of the rotation rate, j_{max}^{-1} vs. $\omega^{-1/2}$. This relationship is given by the following expression [15],

$$\frac{1}{j_{\max}(\omega)} = \frac{1}{j_{\max}^{kin}} + \left(\frac{f_{aa}}{B}\right)\frac{1}{\omega^{1/2}} \tag{2}$$

where j^{kin}_{max} is the limiting kinetic current density of the Tafel step, which represents the mixed behaviour of the hydrogen oxidation, with simultaneous kinetic and diffusion contributions, and B is the Levich constant. Therefore, the constants f_{aa}/B and j^{kin}_{max} can be obtained from the slope and the origin ordinate of the experimental plot j^{-1}_{max} vs. $\omega^{-1/2}$. Fig. 6 illustrates such plot, where it can be observed that the experimental points (dots) satisfy the required linearity. From linear regression (line) the following values were obtained: $(j^{kin}_{max})^{-1} = 247.26$ A^{-1} cm^2 and $f_{aa}/B = 140895.6$ A^{-1} cm^2 rpm$^{1/2}$. From this value, the constant B can be evaluated: $B = 1.042 \times 10^{-4}$ A cm^{-2} rpm$^{-1/2}$.

The experimental polarization resistance $Rp(\omega)$ can be also evaluated from the dependences $j(\eta, \omega)$ near equilibrium, which must satisfy the following linear expression on $\omega^{-1/2}$ [10],

$$Rp(\omega) = Rp^o + \frac{RT}{2F}\frac{f_{aa}}{B}\frac{1}{\omega^{1/2}} \tag{3}$$

From the origin ordinate of the plot $Rp(\omega)$ vs. $\omega^{-1/2}$ (Fig. 7), the value of the equilibrium polarization resistance (Rp^o) was obtained: $Rp^o = 136{,}7\ \Omega\ \text{cm}^2$. Moreover, from the slope of the straight line, which value is 1858.2 Ω cm^2 rpm$^{1/2}$, the constant B can be also evaluated. The value obtained is B = 1.015×10^{-4} A cm^{-2} rpm$^{-1/2}$, which is quite similar to that calculated from Fig. 6. This result evidences the self consistency between the experimental results and the kinetic mechanism.

Finally, the experimental dependence $j(\eta, \omega)$ were described in the whole range of overpotentials with the kinetic expression resulting from the rigorous resolution of the kinetic mechanism on steady state, considering a Frumkin type adsorption of the reaction intermediate. Details of the resolution, which considers the simultaneous occurrence of the two independent routes, Tafel-Volmer and Heyrovsky-Volmer, can be found elsewhere [16]. One of the three equivalent expressions for $j(\eta, \omega)$ is,

$$j = \frac{\nu^e_H e^{-u(\theta-\theta^e)\lambda} e^{\alpha_H f\eta}\left[\frac{(1-\theta)}{(1-\theta^e)} - \frac{\theta e^{-f\eta} e^{u(\theta-\theta^e)}}{\theta^e}\right] + \nu^e_T e^{-2u(\theta-\theta^e)\lambda}\left[\frac{(1-\theta)^2}{(1-\theta^e)^2} - \frac{\theta^2 e^{2u(\theta-\theta^e)}}{\theta^{e2}}\right]}{\frac{1}{2F} + \frac{\nu^e_T f_{aa}(1-\theta)^2 e^{-2u(\theta-\theta^e)\lambda}}{B\omega^{1/2}(1-\theta^e)^2} + \frac{\nu^e_H f_{aa}(1-\theta) e^{-u(\theta-\theta^e)\lambda} e^{\alpha_H f\eta}}{B\omega^{1/2}(1-\theta^e)}} \tag{4}$$

The implicit equation for the variation of the surface coverage (θ) of the reaction intermediate on overpotential is given by,

$$\left\{\nu^e_V e^{-u(\theta-\theta^e)\lambda} e^{\alpha_V f\eta}\left[\frac{\theta e^{u(\theta-\theta^e)}}{\theta^e} - \frac{(1-\theta)e^{-f\eta}}{(1-\theta^e)}\right] + \nu^e_H e^{-u(\theta-\theta^e)\lambda} e^{\alpha_H f\eta}\left[\frac{(1-\theta)}{(1-\theta^e)} - \frac{\theta e^{-f\eta} e^{u(\theta-\theta^e)}}{\theta^e}\right]\right\} \times \left\{\frac{1}{2F} + \frac{\nu^e_T f_{aa}(1-\theta)^2 e^{-2u(\theta-\theta^e)\lambda}}{B\omega^{1/2}(1-\theta^e)^2}\right\}$$
$$- \left\{\frac{1}{F} + \frac{\nu^e_H f_{aa}(1-\theta) e^{-u(\theta-\theta^e)\lambda} e^{\alpha_H f\eta}}{B\omega^{1/2}(1-\theta^e)}\right\} \times \left\{\nu^e_V e^{-u(\theta-\theta^e)\lambda} e^{\alpha_V f\eta}\left[\frac{\theta e^{u(\theta-\theta^e)}}{\theta^e} - \frac{(1-\theta)e^{-f\eta}}{(1-\theta^e)}\right] - \nu^e_T e^{-2u(\theta-\theta^e)\lambda}\left[\frac{(1-\theta)^2}{(1-\theta^e)^2} - \frac{\theta^2 e^{2u(\theta-\theta^e)}}{\theta^{e2}}\right]\right\} = 0 \tag{5}$$

In Eqs. (4) and (5), ν_i is the reaction rate of the step i (i = T, H, V), α_i (i = V,H) is the symmetry factor of the step i, λ is the symmetry factor of adsorption and u (in RT units) is the energy of interaction between the adsorbed hydrogen atoms. Superscript e indicates equilibrium and $f = F/RT$. The experimental $j(\eta)$ curves for each ω value were correlated using Eqs. (4) and (5), applying a non linear least squares regression method. The value $f_{aa}/B = 140895.6$ A^{-1} cm^2 rpm$^{1/2}$ was used in the correlation, while to the symmetry factors α_V and α_H were assigned the value 0.5. Besides, from the definition of the limiting kinetic current density of the Tafel step [15],

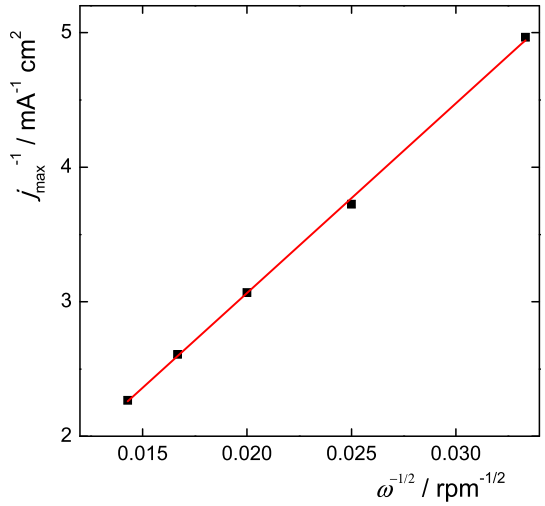

Fig. 6. j^{-1}_{max} vs. $\omega^{-1/2}$ plot. Experimental (symbols), linear regression (line).

$$j^{kin}_{max} = \frac{2F\nu^e_T e^{2\lambda u\theta^e}}{(1-\theta^e)^2} \tag{6}$$

and the value obtained from Fig. 6 ($j^{kin}_{max} = 4.044 \cdot 10^{-3}$ A cm^{-2}), the following expression for the equilibrium reaction rate of the Tafel step is obtained,

$$\nu^e_T\left[\text{mol cm}^{-2}\text{s}^{-1}\right] = 2.096 \times 10^{-8}(1-\theta^e)^2 e^{-2\lambda u\theta^e} \tag{7}$$

Thus, the adjustable parameters for the correlation were ν^e_V, ν^e_H,

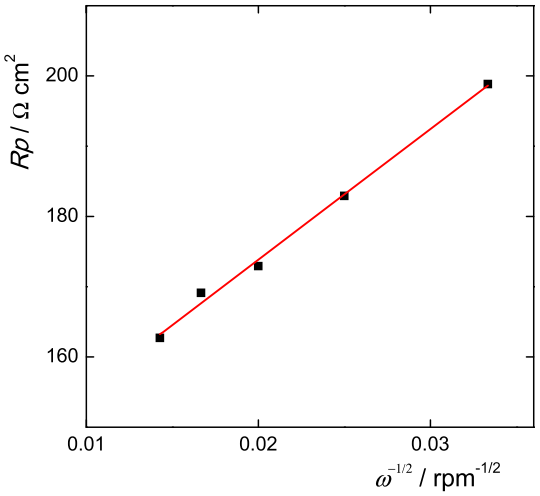

Fig. 7. Rp vs. $\omega^{-1/2}$ plot. Experimental (symbols), linear regression (line).

θ^e, u and λ. They were obtained from the correlation of the experimental curve $j(\eta)$ obtained at $\omega = 4900$ rpm. The values obtained are $\nu_V^e = 2.667 \times 10^{-9}$ mol cm^{-2} s^{-1}, $\nu_H^e = 1.461 \times 10^{-16}$ mol cm^{-2} s^{-1}, $\theta^e = 0.232$, $u = 11.47$ and $\lambda = 0.45$. Then, from Eq. (7) it was obtained $\nu_T^e = 1.128 \times 10^{-9}$ mol cm^{-2} s^{-1}. The simulations of the dependences $j(\eta, \omega)$ for all experimental rotation rates were carried out with this set of parameters. The corresponding curves are shown in Fig. 5 (lines). It can be appreciated that there is a good agreement between the experimental and simulated curves. It can be also observed that, in the analyzed potential range, the hydrogen oxidation is verified preferentially through the Tafel-Volmer route, with a minor contribution of the Heyrovsky-Volmer route.

The equilibrium reaction rates of the three elementary steps obtained from the correlation can be compared with those evaluated in acid solution [16]. The values calculated in 0.5 M H_2SO_4 were: $\nu_V^e = 4.60 \times 10^{-9}$ mol cm^{-2} s^{-1}, $\nu_H^e = 6.0 \times 10^{-9}$ mol cm^{-2} s^{-1} and $\nu_T^e = 1.27 \cdot 10^{-9}$ mol cm^{-2} s^{-1}. It can be observed that the values corresponding to ν_V^e and ν_T^e are quite similar to those found in alkaline solution. On the contrary, the equilibrium reaction rate of the Heyrovsky step is eight orders of magnitude lower than that in sulphuric acid solution. Taking into account that the influence of hydroxide concentration is the same for ν_V^e and ν_H^e [25], it would be expected a similar behaviour for both kinetic parameters. Moreover, the lower value of ν_H^e cannot be ascribed to the inhibition of active sites due to the adsorption of OH because it would have affected all the equilibrium reaction rates. The strong inhibition of the Heyrovsky step in alkaline solutions could be explained on the basis of the structure of the water layer adjacent to the electrodic surface. It can be considered a highly ordered water network as a consequence of the strong interaction with the metal surface. As the Heyrovsky step requires the reaction between hydroxide ion and molecular hydrogen in the reaction plane, OH^- species must migrate through the superficial water network towards the surface. This motion should be verified through a Grotthuss type process, with the hydroxide ion accepting and donating hydrogen bond from and to water molecules. As both, water molecules and hydroxide ion, vibrate around quasistatic positions, the transference of the hydrogen bond would take place when they are in an adequate spatial configuration. Moreover, when OH ions get the reaction plane at the network–electrode interface, its reaction with the hydrogen molecule will be also determined by their relative spatial position, which must be appropriate for the electron and hydrogen transfer needed by the Heyrovsky step. Consequently, the results obtained would indicate that these conditions are not fulfilled due to the high interaction with water network. On the other hand, in acid solutions the situation is different because in this case the direct decomposition of molecular hydrogen produces H^+ ions, which have less spatial restrictions, justifying a higher reaction rate for this step. This hypothesis needs to be ratified through the analysis of the hor on other metals in alkaline solution. The inhibition of the Heyrovsky step is clearly undesired, as the occurrence of the hydrogen oxidation through the Tafel-Volmer route is more inefficient [26]. This aspect should be investigated, as the performance of the hor could be improved by changing the solvent and thus making the reaction to proceed under the Heyrovsky-Volmer route.

3.4. Electrocatalytic activity

The electrocatalytic activity of a given electrode material for the hydrogen electrode reaction is represented usually by the exchange current density, which is related to the kinetic parameters by the following equation [26,27],

$$j_o = 2F\left(\frac{\nu_T^e\nu_V^e + \nu_H^e\nu_V^e + \nu_T^e\nu_H^e}{(\nu_V^e + \nu_H^e + 2\nu_T^e)}\right) \quad (8)$$

The value obtained from the equilibrium reaction rates of the elementary steps evaluated from the correlation of the experimental results is $j_o = 1.18 \times 10^{-4}$ A cm^{-2}, which is slightly lower than that obtained for rhodium in acid solution (6.77×10^{-4} A cm^{-2}) [16].

4. Conclusions

The hydrogen oxidation reaction was studied on a rotating disc electrode of nanostructured rhodium supported on glassy carbon, being the electroactive area evaluated by CO stripping voltammetry. The kinetic parameters resulting from the rigorous resolution of the Tafel-Heyrovsky-Volmer mechanism were evaluated from the correlation of the experimental current density–overpotential curves measured at different rotation rates in the overpotential range $-0.15 < \eta/V < 0.40$. It was demonstrated that in the analyzed overpotential region the reaction takes place preferentially through the Tafel-Volmer route and to a lesser extent through the Heyrovsky-Volmer route. The exchange current density was also evaluated from these kinetic parameters.

Acknowledgements

The authors wish to acknowledge the financial support received from ANPCyT, CONICET and UNL.

References

[1] A.F. Inocente, A.C.D. Angelo, J. Power Sources 162 (2006) 151–159.
[2] K. Kanimatsu, H. Uchida, M. Osawa, M. Watanabe, J. Electroanal. Chem. 587 (2006) 299–307.
[3] I. Esparbé, E. Brillas, F. Centellas, J.A. Garrido, R.M. Rodriguez, C. Arias, P.L. Cabot, J. Power Sources 190 (2009) 201–209.
[4] M. Wesselmark, B. Wickman, C. Lagergren, G. Lindbergh, Electrochem. Commun. 12 (2010) 1585–1588.
[5] S.N. Pronkin, A. Bonnefont, P.S. Ruvinskiy, E.R. Savinova, Electrochim. Acta 55 (2010) 3312–3323.
[6] Y. Sun, Y. Dai, Y. Liu, S. Chen, Phys. Chem. Chem. Phys. 14 (2012) 2278–2285.
[7] A.N. Simonov, P.E. Plyusnin, Y.V. Shubin, R.I. Kvon, S.V. Korenev, V.N. Parmon, Electrochim. Acta 76 (2012) 344–353.
[8] A. Bonnefont, A.N. Simonov, S.N. Pronkin, E.Y. Gerasimov, P.A. Pyrjaev, V.N. Parmon, E.R. Savinova, Catal. Today 202 (2013) 70–78.
[9] M.R. Gennero de Chialvo, A.C. Chialvo, Phys. Chem. Chem. Phys. 6 (2004)

4009–4017.
[10] P.M. Quaino, M.R. Gennero de Chialvo, A.C. Chialvo, Phys. Chem. Chem. Phys. 6 (2004) 4450–4455.
[11] P.M. Quaino, J.L. Fernández, M.R. Gennero de Chialvo, A.C. Chialvo, J. Mol. Catal. A Chem. 252 (2006) 156–162.
[12] M.S. Rau, P.M. Quaino, M.R. Gennero de Chialvo, A.C. Chialvo, Electrochem. Commun. 10 (2008) 208–212.
[13] M.S. Rau, M.R. Gennero de Chialvo, A.C. Chialvo, Electrochim. Acta 55 (2010) 5014–5018.
[14] M.S. Rau, M.R. Gennero de Chialvo, A.C. Chialvo, J. Power Sources 229 (2013) 210–215.
[15] M.A. Montero, J.L. Fernández, M.R. Gennero de Chialvo, A.C. Chialvo, J. Phys. Chem. C 117 (2013) 25269–25275.
[16] M.A. Montero, J.L. Fernández, M.R. Gennero de Chialvo, A.C. Chialvo, J. Power Sources 254 (2014) 218–223.
[17] J.A. Harrison, Z.A. Khan, J. Electroanal. Chem. 30 (1971) 327–330.
[18] V.S. Bagotzky, N.V. Osetrova, J. Electroanal. Chem. 43 (1973) 233–249.
[19] G. Couturier, D.W. Kirk, P.J. Hyde, S. Srinivasan, Electrochim. Acta 32 (1987) 995–1005.
[20] T.J. Schmid, P.N. Ross Jr., N.M. Markovic, J. Electroanal. Chem. 524–525 (2002) 252–260.
[21] Z. Cataldi, R.O. Lezna, M.C. Giordano, A.J. Arvia, J. Electroanal. Chem. 261 (1988), 61–15.
[22] J. Ohyama, T. Sato, Y. Yamamoto, S. Arai, A. Satsuma, J. Am. Chem. Soc. 135 (2013) 8016–8021.
[23] B. Losiewicz, R. Jurczakowski, A. Lasia, Electrochim. Acta 56 (2011) 5746–5753.
[24] X.F. Lin, B. Ren, Z.Q. Tian, J. Phys. Chem. B 108 (2004) 981–986.
[25] J.L. Fernandez, M.R. Gennero de Chialvo, A.C. Chialvo, Phys. Chem. Chem. Phys. 5 (2003) 2875–2880.
[26] M.R. Gennero de Chialvo, A.C. Chialvo, J. Electroanal. Chem. 415 (1996) 97–106.
[27] M.R. Gennero de Chialvo, A.C. Chialvo, Curr. Top. Electrochem. 17 (2012) 41–52.